

The form factors of the nucleon at small momentum transfer

Véronique Bernard^{a*}, Harold W. Fearing^{b†}, Thomas R. Hemmert^{b‡§} and Ulf-G. Meißner^{c**}

^a *Laboratoire de Physique Théorique, BP 28, F-67037 Strasbourg Cedex 2, France*

^b *Theory Division, TRIUMF, 4004 Wesbrook Mall, Vancouver, BC, Canada V6T 2A3*

^c *Forschungszentrum Jülich, Institut für Kernphysik (Th), D-52425 Jülich, Germany*

We study the low energy expansion of the nucleon's electroweak form factors in the framework of an effective chiral Lagrangian including pions, nucleons and the $\Delta(1232)$. We work to third order in the so-called small scale expansion and compare the results with the ones previously obtained in the chiral expansion. In addition, these calculations serve as a first exploratory study of renormalization and decoupling within the small scale expansion.

*email: bernard@sbghp4.in2p3.fr

†email: fearing@triumf.ca

‡email: hemmert@triumf.ca

§Address after February 1st, 1998: FZ Jülich, IKP (Th), D-52425 Jülich.

**email: Ulf-G.Meissner@fz-juelich.de

I. INTRODUCTION AND SUMMARY

The electromagnetic and axial structure of the nucleon as revealed e.g. in elastic electron–nucleon and (anti)neutrino–nucleon scattering as well as in charged pion electroproduction is parameterized in terms of the six form factors $F_{1,2}^{p,n}(q^2)$ and $G_{A,P}(q^2)$ (with q^2 the squared momentum transfer). The understanding of these form factors is of utmost importance in any theory or model of the strong interactions. At low energies, these form factors can be Taylor expanded in q^2 , with the terms linear in q^2 giving the respective charge, magnetic and axial radii. It should not come as a surprise that these different probes, i.e. the isoscalar/isovector vector and the isovector axial current, see different nucleon sizes. While the electromagnetic radii have a typical size of about 0.85 fm, the axial radius is significantly smaller, about 0.65 fm. The pattern of these scales is related to the various intermediate states dominating the response of an isoscalar/isovector photon or the external axial current (mediated by the W/Z -bosons) (for a very instructive model, see [1]). The current situation concerning the theoretical understanding and experimental knowledge of the electromagnetic form factors is reviewed in [2] [3] [4].

Chiral perturbation theory (ChPT) can be used to investigate the Green functions of QCD quark currents in the low energy domain. The abovementioned form factors have been studied over the years in the relativistic formulation of baryon ChPT [5] and in the heavy baryon formulation (HBChPT), which admits a one-to-one correspondence between the expansion in pion loops on one side and small momenta and quark (pion) masses on the other [6]. Here small means with respect to a typical hadronic scale, say the proton mass. In addition, the spectral functions of the isoscalar electromagnetic as well as the isovector axial current have been worked out to two loop accuracy [7]. This is mandated by the fact that in a dispersive representation, the pertinent absorptive parts start to contribute with the three-pion intermediate state and are therefore not accessible in a one-loop calculation. It could also be shown that the strong unitarity correction on the left wing of the ρ -resonance in the isovector electromagnetic channel can be reproduced by a one loop calculation [5] [7]. Furthermore, the relation between the axial radius extracted from (anti)neutrino–proton scattering or pion electroproduction data was clarified in [8] and precise predictions for the induced pseudoscalar coupling constant g_P were made in Refs. [9] [10].

It has been argued for some time that for baryon ChPT, one has to include the spin-3/2 decuplet (in $SU(3)$) or the $\Delta(1232)$ (in $SU(2)$) [11].¹ This is motivated by the close proximity of this nucleon resonance to the ground state and its very strong coupling to the pion–nucleon–photon system. In fact, for QCD in the limit of infinitively many colors, the nucleon and the delta resonance become degenerate in mass. Therefore, in Refs. [12] [13] the so-called small scale expansion was developed. Besides the two small parameters known from the chiral expansion, the $N\Delta$ mass splitting Δ is introduced as an additional small parameter and the methods of [6] have been generalized to deal with such a situation. These three expansion parameters are collectively called ϵ . To assess the accuracy of this novel approach and compare it to the conventional chiral expansion, one has to systematically calculate observables and compare the resulting predictions. Here, we concentrate on the aforementioned form factors for essentially two reasons. First, these are relatively simple three-point functions and they are known empirically to a good precision. Second, this work contains the first exploratory study of $\mathcal{O}(\epsilon^3)$ renormalization in the small scale expansion. This latter topic is only in its infant stage and many more details will have to be worked out.

The pertinent results of this investigation can be summarized as follows:

- 1) We have constructed the complete $\pi N \Delta \gamma$ effective Lagrangian necessary to investigate the nucleons electroweak form factors in the small scale expansion to order ϵ^3 . In particular, we have performed the necessary renormalization of the nucleon mass and various coupling constants, cf. Table 1. We have also discussed the decoupling of the delta degrees of freedom and how it affects the finite values of certain new counterterms related to the new scale Δ .
- 2) We have considered in detail the isovector nucleon form factors at small momentum transfer. We recover the well-known result that the radii corresponding to the Dirac and Pauli form factor explode in the chiral limit like $\log m_\pi$ and $1/m_\pi$, respectively. The new delta contributions bring the prediction for the Pauli radius r_2^v closer to the empirical value and lead to an improved description of the Pauli form factor for momentum transfer $|q^2| \leq 0.2 \text{ GeV}^2$, cf. Fig. 2. The Dirac form factor as given by the chiral and the small scale expansion agrees nicely with result based on dispersion relations.

¹From now on, we will only be concerned with the two flavor case.

- 3) The results for the isoscalar electromagnetic form factors differ from the ones in the chiral expansion only by a finite counterterm, which has no physical consequence. Combining these with the isovector form factors, the corresponding electric and magnetic proton form factors, as well as the magnetic neutron one, come rather close to the empirical dipole fit. The prediction for the neutron charge form factor is somewhat smaller than the best available parameterizations but consistent with the rather uncertain data (below $|q^2| \leq 0.1 \text{ GeV}^2$), see figs.3a,b.
- 4) The axial form factor $G_A(q^2)$ receives only polynomial terms up-to-and-including order q^2 in the momentum expansion. As in the case of the chiral expansion, the axial radius is determined by a finite low-energy constant. Delta effects only appear in the renormalization of the axial-vector coupling constant $g_A \equiv G_A(0)$ but do not affect the q^2 dependence of this form factor to the order we are working.
- 5) The prediction for the induced pseudoscalar form factor $G_P(q^2)$ and the coupling constant g_P as well as the so-called Goldberger-Treiman discrepancy are also found not to be affected by the delta to leading order in the small scale expansion, once the renormalization of the coupling constants has been accounted for (see table 2). $\Delta(1232)$ effects in the individual weak and electromagnetic form factors can therefore not explain the recently published TRIUMF value for g_P obtained from a measurement of radiative muon capture [14]. Other $\Delta(1232)$ effects in radiative muon capture are also apparently small [15].

II. HBCHPT AND THE SMALL SCALE EXPANSION

A. Effective Lagrangian, renormalization and decoupling

In this section, we give the effective Lagrangian of the pion-nucleon- $\Delta(1232)$ -photon system necessary to work out the nucleon's electroweak form factors at low energies. The chiral counting is supplemented by an additional small parameter, the $\Delta(1232)$ -nucleon mass splitting $M_\Delta - M_N$, denoted as Δ . In contrast to the external momenta (p) and the pion mass (m_π), this quantity does not vanish in the chiral limit of QCD. However, for a very large number of colors, the nucleon and the $\Delta(1232)$ become degenerate in mass. Furthermore, the Δ -resonance is very strongly coupled to the $\pi N \gamma$ system. One therefore considers an expansion in a small parameter ϵ , which in fact is a triple expansion, since

$$\epsilon \in \{p, m_\pi, \Delta\} . \quad (1)$$

All these are small quantities compared to the typical hadronic scale of about 1 GeV. This extends the chiral expansion in a logical fashion for such resonance degrees of freedom. It should, however, be kept in mind that we are not dealing with a low-energy expansion in the strict sense, where all expansion parameters vanish in a certain limit. For more details, we refer the reader to [12], [13].

Consider first the lowest order Lagrangians of dimension one and two. These are special since loops only start at dimension three and thus the pertinent coupling constants are not affected by loop effects to this order and are therefore finite. Denoting by N the (heavy) nucleon isodoublet field and by T_λ^i the Rarita-Schwinger representation of the (heavy) spin-3/2 field (the delta), we have

$$L_{\pi N}^{(1)} = \bar{N}(i v \cdot D + \dot{g}_A S \cdot u)N , \quad (2)$$

$$L_{\pi \Delta}^{(1)} = -\bar{T}_\mu^i (i v \cdot D^{ij} - \Delta_0 \xi_{3/2}^{ij} + \dot{g}_1 S \cdot u^{ij}) g^{\mu\nu} T_\nu^j , \quad (3)$$

$$L_{\pi N \Delta}^{(1)} = \dot{g}_{\pi N \Delta} \bar{T}_\mu^i w_i^\mu N + \text{h.c.} , \quad (4)$$

$$L_{\pi N}^{(2)} = \bar{N} \left\{ \frac{1}{2M_0} (v \cdot D)^2 - \frac{1}{2M_0} D \cdot D - \frac{i \dot{g}_A}{2M_0} \{ S \cdot D, v \cdot u \} + c_1 \text{Tr}(\chi_+) \right. \\ \left. - \frac{i}{4M_0} [S^\mu, S^\nu] \left[(1 + \dot{\kappa}_v) f_{\mu\nu}^+ + 2(1 + \dot{\kappa}_s) v_{\mu\nu}^{(s)} \right] + \dots \right\} N . \quad (5)$$

The ellipsis denotes other terms not relevant for the further discussion. Here, \dot{Q} denotes that a quantity Q is taken in the chiral SU(2) limit,² $m_u = m_d = 0$ and m_s fixed, i.e.

²The exception to this are the nucleon mass, the $N\Delta$ -splitting and the pion decay constant in the chiral limit, which are denoted by M_0 , Δ_0 and F_0 , respectively. To the accuracy we are working, we can set $\Delta_0 = \Delta$.

$$Q = \dot{Q} [1 + \mathcal{O}(m_{u,d}^\alpha)] , \quad (6)$$

with the power $\alpha = 1/2$ or 1. Furthermore, $i, j = 1, 2, 3$ are isospin indices, $\xi_{3/2}^{ij}$ is an isospin-3/2 projection operator, D_μ^{ij} is the covariant derivative for spin 3/2, isospin 3/2 systems [12,13] and S_μ is the Pauli–Lubanski spin vector. We also employ

$$w_\mu^i = \frac{1}{2} \text{Tr} (\tau^i u_\mu) , \quad (7)$$

$$u_\mu^{ij} = \xi_{3/2}^{ik} u_\mu \xi_{3/2}^{kj} . \quad (8)$$

The scalar source χ_+ includes the explicit chiral symmetry breaking through the pion mass m_π and $\kappa_{s,v}$ are the isoscalar/isovector anomalous magnetic moments of the nucleon. We follow here the notation of [16], i.e. the isovector component of the photon is encoded in $f_{\mu\nu}^+$ whereas the isoscalar sources are contained in $v_{\mu\nu}^{(s)}$. For more details, we refer the reader to Refs. [16] [17] (nucleon sector) and Refs. [12] [13] ($N\Delta$ sector). Throughout, we use $g_{\pi N\Delta} = 1.05$, $g_A = 1.26$, $M_N = 0.938$ GeV, $m_\pi = 0.14$ GeV, $F_\pi = 0.0925$ GeV and $\Delta = 0.294$ GeV. The $\Delta\Delta\pi$ coupling constant g_1 appears only in the renormalization of g_A (cf. Table 2) and we therefore do not need to specify its value.

At order ϵ^3 , there are two types of contributions. First, there are $1/M_N^2$ corrections with fixed coefficients. These can be deduced in the standard fashion from the lagrangian,

$$L_{\pi N}^{(3),\text{fixed}} = \bar{N} \left[\gamma_0 \tilde{\mathcal{B}}_N^\dagger \gamma_0 \tilde{\mathcal{C}}_N^{-1} \tilde{\mathcal{B}}_N + \gamma_0 \mathcal{B}_{\Delta N}^\dagger \gamma_0 \mathcal{C}_{\Delta}^{-1} \mathcal{B}_{\Delta N} \right] N , \quad (9)$$

with the explicit form of the various matrices $\tilde{\mathcal{B}}_N, \mathcal{B}_{\Delta N}, \dots$ given in [13]. Second, the $\mathcal{O}(\epsilon^3)$ counterterms are given by the general structure (the explicit form of the operators is given in the later sections)

$$\begin{aligned} L_{\pi N}^{(3)} = & \frac{1}{(4\pi F_\pi)^2} \sum_{i=1}^{22} B_i \bar{N} O_i^{(3)} N + \frac{1}{(4\pi F_\pi)^2} \sum_{j=1}^9 \tilde{B}_j \bar{N} O_j^{(3)} N \\ & + \frac{\Delta}{(4\pi F_\pi)^2} \sum_{i=23}^{29} B_i \bar{N} O_i^{(2)} N + \frac{\Delta^2}{(4\pi F_\pi)^2} \sum_{i=30}^{31} B_i \bar{N} O_i^{(1)} N + \frac{\Delta^3}{(4\pi F_\pi)^2} B_{32} \bar{N} O_{32}^{(0)} N , \end{aligned} \quad (10)$$

with

$$\begin{aligned} B_i &= B_i^r(\lambda) + \beta_i 16\pi^2 L , \\ L &= \frac{\lambda^{d-4}}{16\pi^2} \left[\frac{1}{d-4} + \frac{1}{2} (\gamma_E - 1 - \ln 4\pi) \right] , \end{aligned} \quad (11)$$

with γ_E the Euler–Mascheroni constant and λ the scale of dimensional regularization. The β -functions β_i ($i = 1, 22$) for the nucleon sector are tabulated in [18]. The additional finite terms \tilde{B}_j are scale-independent and can be found in [19]. We note that in principle there are ten³ new counterterms [13] in Eq.(10) in addition to the 22 counterterms of $\mathcal{O}(p^3)$ HBChPT [18] and the 9 finite terms at $\mathcal{O}(p^3)$ [19]⁴. However, the 10 new counterterms in the nucleon sector are unobservable in the sense that they do not bring about any new vertices for the theory as they correspond to lower order HBChPT Lagrangians multiplied with the new scale Δ . They will therefore always enter in combinations with Δ independent couplings or counterterms (see Table 2) and we could choose their finite parts $B_i^r(\lambda)|_{i=23\dots 32}$ in order to guarantee decoupling of the delta-resonance in the limit $\Delta \rightarrow \infty$ without affecting measurable quantities. Nevertheless, throughout this work we will choose to write all results in terms of physical coupling constants and therefore completely avoid the question of the finite sizes for these terms. Once our results are written in terms of physical quantities the decoupling of $\Delta(1232)$ contributions in the limit $\Delta \rightarrow \infty$ must of course be “automatically” guaranteed. For a general discussion of decoupling in the effective meson–baryon field theory we refer to [20,21] and will come back to this point later. In Table 1 we have collected the counterterm structures which are of relevance for the problem under consideration. We give the pertinent operators together with their β functions in the chiral and in the small scale expansion, to order p^3 and ϵ^3 , respectively, and indicate in which quantity they appear.

³Our analysis will suggest that B_{29} is finite, see Table 1.

⁴We note that by construction the $\mathcal{O}(\epsilon^n)$ “small scale expansion” has been set up that one can recover both the $\mathcal{O}(p^n)$ HBChPT lagrangians and the $\mathcal{O}(p^n)$ results in the “limit” where all $\Delta(1232)$ dependent couplings are set to zero.

B. Nucleon mass and wave function renormalization

We only need the leading term in the renormalization of the nucleon mass which is not modified by delta degrees of freedom:

$$M_N = M_0 - 4c_1 m_\pi^2 + \mathcal{O}(\epsilon^3) , \quad (12)$$

where the LEC c_1 can e.g. be extracted from the pion–nucleon σ -term. Note that at order ϵ^3 , the dimension zero operator $O_{32}^{(0)}$ leads to a finite shift of the nucleon mass in the chiral limit. For the deltas treated relativistically, this shift is known to be infinite [22]. For a more detailed study of the nucleon mass in the small scale expansion we refer to the talk by Kambor [23]. The nucleon wave function renormalization constant Z_N to $\mathcal{O}(\epsilon^3)$ reads

$$Z_N^{(3)} = 1 - \frac{1}{(4\pi F_\pi)^2} \left\{ \left(\frac{3}{2} g_A^2 + 4g_{\pi N\Delta}^2 \right) m_\pi^2 - 16g_{\pi N\Delta}^2 \Delta \sqrt{\Delta^2 - m_\pi^2} \log R \right. \\ \left. + 8m_\pi^2 B_{20}^r(\lambda) + \left(\frac{9}{2} g_A^2 m_\pi^2 + 8g_{\pi N\Delta}^2 m_\pi^2 \right) \log \left[\frac{m_\pi}{\lambda} \right] + \Delta^2 B_{30}^r(\lambda) - 16g_{\pi N\Delta}^2 \Delta^2 \log \left[\frac{m_\pi}{\lambda} \right] \right\} , \quad (13)$$

with

$$R = \frac{\Delta}{m_\pi} + \sqrt{\frac{\Delta^2}{m_\pi^2} - 1} = 3.95 . \quad (14)$$

In this and most subsequent formulas, to the order required, all couplings, mass terms and decay constants have been expressed in terms of their *physical* values as detailed in Table 2. We note that some authors employ additional momentum-dependent terms in Z_N (see e.g. the discussion in refs. [10,24]), which we have chosen to be absorbed in the relativistic normalization of our nucleon spinors. Physical results, of course, do not depend on this choice, as the nucleon Z -factor is not a measurable quantity but only needed to perform the necessary renormalizations.

III. ISOVECTOR VECTOR FORM FACTORS

The structure of the nucleon probed with virtual photons is encoded in two form factors, called $F_{1,2}(q^2)$, with q^2 the squared four-momentum transfer. Since the photon itself has an isoscalar and an isovector component, it is natural to decompose these form factors into corresponding isoscalar/isovector (s/v) parts. In this section, we are concerned with the isovector form factors. To one loop, these encode more information than their isoscalar counterparts because the pertinent spectral functions start with the two-pion cut and thus lead to a non-polynomial contribution at this order.

A. Definition

Consider the nucleon matrix element of the isovector component of the quark vector current $V_\mu^i = \bar{q}\gamma_\mu(\tau^i/2)q$, which involves a vector and a tensor form factor,

$$\langle N(p_2) | V_\mu^i(0) | N(p_1) \rangle = \bar{u}(p_2) \left[F_1^v(q^2) \gamma_\mu + \frac{i}{2M_N} F_2^v(q^2) \sigma_{\mu\nu} q^\nu \right] u(p_1) \times \eta^\dagger \frac{\tau^i}{2} \eta , \quad (15)$$

where $u(p)$ is a Dirac spinor with isospin component η and $q^2 = (p_2 - p_1)^2$ is the invariant momentum transfer squared. $F_1(q^2)$ and $F_2(q^2)$ are the Dirac and the Pauli form factor, respectively, subject to the normalizations

$$F_1^v(0) = 1 , \quad F_2^v(0) = \kappa_v , \quad (16)$$

with $\kappa_v = 3.71$ the isovector nucleon anomalous magnetic moment. As pointed out in [6], in the heavy baryon approach it is most natural to work in the brick-wall (Breit) frame since the nucleons (and also the deltas) are essentially heavy static sources. Furthermore, the Breit frame allows for a unique translation of the Lorentz-covariant matrix elements into non-relativistic ones. Thus performing the non-relativistic reduction in the Breit frame and utilizing the heavy-mass decomposition

$$p_1^\mu \rightarrow M_0 v^\mu + r_1^\mu, \quad p_2^\mu \rightarrow M_0 v^\mu + r_2^\mu, \quad (17)$$

one obtains

$$\langle N(p_2) | V_\mu^i(0) | N(p_1) \rangle = \frac{1}{N_1 N_2} \bar{u}_v(r_2) \left[\tilde{G}_E^v(q^2) v_\mu + \frac{1}{M_N} \tilde{G}_M^v(q^2) [S_\mu, S_\nu] q^\nu \right] u_v(r_1) \times \eta^\dagger \frac{\tau^i}{2} \eta, \quad (18)$$

with

$$u_v(r) = P_v^+ u(p), \quad P_v^+ = \frac{1}{2} (1 + \not{v}), \quad N_i = \sqrt{\frac{E_i + M_N}{2M_N}}, \quad (i = 1, 2). \quad (19)$$

Here, $r_{1,2}^\mu$ are small (“soft”) momenta in the sense that $r_{1,2}^\mu v_\mu \ll M_0$. For the specific choice $v^\mu = (1, 0, 0, 0)$ of the the velocity vector v_μ they read

$$r_1^\mu = \left(E - M_0, -\frac{\vec{q}}{2} \right), \quad r_2^\mu = \left(E - M_0, +\frac{\vec{q}}{2} \right), \quad q^\mu = (0, \vec{q}) \quad (20)$$

and the form factors $\tilde{G}_E(q^2), \tilde{G}_M(q^2)$ then correspond to the well-known electric, $G_E(q^2)$, and magnetic, $G_M(q^2)$, Sachs form factors. These are connected to the previously defined Dirac/Pauli form factors via

$$G_E^v(q^2) = F_1^v(q^2) + \frac{q^2}{4M_N^2} F_2^v(q^2), \quad (21)$$

$$G_M^v(q^2) = F_1^v(q^2) + F_2^v(q^2). \quad (22)$$

The Sachs form factors are normalized to the isovector electric charge and the isovector total magnetic moment of the nucleon, respectively. We now turn to the chiral expansion of these various isovector form factors.

B. Chiral Input

In Fig.1, the pertinent one loop graphs for the $\mathcal{O}(\epsilon^3)$ calculation are shown. The following pieces of the dimension three chiral Lagrangian are needed,

$$\begin{aligned} \mathcal{L}_{\pi N}^{(3)} = & \frac{1}{(4\pi F_\pi)^2} \bar{N} \{ B_{10} D^\mu f_{\mu\nu}^+ v^\nu + B_{20} (\text{Tr}(\chi_+) i v \cdot D + \text{h.c.}) + B_{28} \Delta i [S^\mu, S^\nu] f_{\mu\nu}^+ + B_{30} \Delta^2 i v \cdot D \} N \\ & + \frac{1}{2M_0} \bar{N} \left(\gamma_0 B_N^{(2)\dagger} \gamma_0 B_N^{(1)} + \gamma_0 B_N^{(1)\dagger} \gamma_0 B_N^{(2)} \right) N - \frac{1}{(2M_0)^2} \bar{N} \gamma_0 B_N^{(1)\dagger} \gamma_0 (i v \cdot D + \not{A} S \cdot u) B_N^{(1)} N. \end{aligned} \quad (23)$$

Here, $B_{10}, B_{20}, B_{28}, B_{30}$ are $\mathcal{O}(\epsilon^3)$ counterterms participating in the renormalization of the loop diagrams 1a...1f. When comparing with the set of infinite counterterms of $\mathcal{O}(p^3)$ HBChPT [18] we note that B_{28}, B_{30} are new counterterms in the nucleon-sector due to the presence of the additional dimensional scale Δ . Note that B_{20} and B_{30} only contribute to the nucleon Z -factor whereas B_{10} and B_{28} are related to the isovector charge radius and the isovector anomalous magnetic moment, see below and Table 2. Finally, the matrices $B_N^{(i)}$ which govern the fixed $1/M^2$ corrections can be found in refs. [6,13].

C. Results

Apart from the loop graphs shown in Fig. 1, one has Born term contributions. Adding these, the electric isovector form factor is given by (see app. A for explicit expressions of the various loop diagrams depicted in Fig. 1)

$$\begin{aligned} G_E^v(q^2) = & 1 + \kappa_v \frac{q^2}{4M_N^2} + \frac{1}{(4\pi F_\pi)^2} \left\{ q^2 \left(\frac{68}{81} g_{\pi N \Delta}^2 - \frac{2}{3} g_A^2 - 2B_{10}^{(r)} \right) + q^2 \left(\frac{40}{27} g_{\pi N \Delta}^2 - \frac{5}{3} g_A^2 - \frac{1}{3} \right) \log \left[\frac{m_\pi}{\lambda} \right] \right. \\ & + \int_0^1 dx \left[\frac{16}{3} \Delta^2 g_{\pi N \Delta}^2 + m_\pi^2 \left(3g_A^2 + 1 - \frac{8}{3} g_{\pi N \Delta}^2 \right) \right. \\ & \left. \left. - q^2 x(1-x) \left(5g_A^2 + 1 - \frac{40}{9} g_{\pi N \Delta}^2 \right) \right] \log \left[\frac{\tilde{m}^2}{m_\pi^2} \right] \right\} \end{aligned}$$

$$\begin{aligned}
& + \int_0^1 dx \left[\frac{32}{9} g_{\pi N \Delta}^2 q^2 x(1-x) \frac{\Delta \log R[\tilde{m}^2]}{\sqrt{\Delta^2 - \tilde{m}^2}} \right] \\
& - \int_0^1 dx \frac{32}{3} g_{\pi N \Delta}^2 \Delta \left[\sqrt{\Delta^2 - m_\pi^2} \log R - \sqrt{\Delta^2 - \tilde{m}^2} \log R[\tilde{m}^2] \right] \Big\} , \quad (24)
\end{aligned}$$

with

$$R[\tilde{m}^2] = \frac{\Delta}{\tilde{m}} + \sqrt{\frac{\Delta^2}{\tilde{m}^2} - 1} , \quad \tilde{m}^2 = m_\pi^2 - q^2 x(1-x) . \quad (25)$$

We note that for the isovector electric form factor, decoupling requires that in the limit $\Delta \rightarrow \infty$ the whole delta contribution can be absorbed in the value of B_{10}^r .

Analogously, the magnetic isovector form factor yields

$$\begin{aligned}
G_M^v(q^2) = & 1 + \kappa_v - g_A^2 \frac{4\pi M_N}{(4\pi F_\pi)^2} \int_0^1 dx \left\{ \sqrt{\tilde{m}^2} - m_\pi \right\} \\
& + \frac{32}{9} g_{\pi N \Delta}^2 \frac{M_N \Delta}{(4\pi F_\pi)^2} \int_0^1 dx \left\{ \frac{1}{2} \log \left[\frac{\tilde{m}^2}{4\Delta^2} \right] - \log \left[\frac{m_\pi}{2\Delta} \right] \right. \\
& \left. + \frac{\sqrt{\Delta^2 - \tilde{m}^2}}{\Delta} \log R[\tilde{m}^2] - \frac{\sqrt{\Delta^2 - m_\pi^2}}{\Delta} \log R \right\} , \quad (26)
\end{aligned}$$

with the renormalization of κ_v given in Table 2. Since the (renormalized) expression for $G_M^v(q^2)$ is free of counterterms, decoupling of the $\Delta(1232)$ for the isovector magnetic form factor demands that as $\Delta \rightarrow \infty$, the delta contributions have to vanish. In addition to the decoupling limit $\Delta \rightarrow \infty$ one can also recover the previously obtained $\mathcal{O}(p^3)$ HBChPT results for $G_E^v(q^2), G_M^v(q^2)$ of [6,10] for the limit $g_{\pi N \Delta} \rightarrow 0$, as promised in footnote 4. To make the comparison with the work of Fearing et al. one must realize that the Ecker-Mojžiš $\mathcal{O}(p^3)$ HBChPT Lagrangian [25] has had some equation-of-motion (EOM) terms transformed away via field-redefinitions, which leads to slightly different expressions for the beta-functions in table 1 and different expressions for the coupling constant renormalizations in table 2. Once one writes the results for the form factors in terms of physical couplings and masses, all these apparent differences of course disappear.

Heavy mass methods like HBChPT or the small scale expansion “naturally” yield non-relativistic results for the quantities of interest. It is therefore the Sachs form factors $G_E(q^2), G_M(q^2)$, which have a simple nonrelativistic physical interpretation, that can be read off directly from the chiral amplitudes expressed in the Breit frame. In order to obtain expressions for the relativistic form factors $F_1^v(q^2), F_2^v(q^2)$ one has to work a little bit. One possible approach consists in casting the heavy baryon amplitudes back into a relativistic form, which was pursued in [10]. In this work we follow a different path. Keeping in mind that the $\mathcal{O}(\epsilon^3)$ calculation is sensitive at most to $1/M_N^2$ structures, one can read off the desired connection via Eq.(22):

$$G_E^v(q^2) = F_1^v(q^2) + \frac{q^2}{4M_N^2} F_2^v(0) + \mathcal{O}(1/M_N^3) \quad (27)$$

$$\frac{1}{M_N} G_M^v(q^2) = \frac{1}{M_N} F_1^v(0) + \frac{1}{M_N} F_2^v(q^2) + \mathcal{O}(1/M_N^3) \quad (28)$$

Therefore, the $\mathcal{O}(\epsilon^3)$ expressions of the Dirac and Pauli form factors read

$$\begin{aligned}
F_1^v(q^2) = & 1 + \frac{1}{(4\pi F_\pi)^2} \left\{ q^2 \left(\frac{68}{81} g_{\pi N \Delta}^2 - \frac{2}{3} g_A^2 - 2B_{10}^{(r)} \right) + q^2 \left(\frac{40}{27} g_{\pi N \Delta}^2 - \frac{5}{3} g_A^2 - \frac{1}{3} \right) \log \left[\frac{m_\pi}{\lambda} \right] \right. \\
& + \int_0^1 dx \left[\frac{16}{3} \Delta^2 g_{\pi N \Delta}^2 + m_\pi^2 \left(3g_A^2 + 1 - \frac{8}{3} g_{\pi N \Delta}^2 \right) \right. \\
& \quad \left. \left. - q^2 x(1-x) \left(5g_A^2 + 1 - \frac{40}{9} g_{\pi N \Delta}^2 \right) \right] \log \left[\frac{\tilde{m}^2}{m_\pi^2} \right] \right. \\
& + \int_0^1 dx \left[\frac{32}{9} g_{\pi N \Delta}^2 q^2 x(1-x) \frac{\Delta \log R[\tilde{m}^2]}{\sqrt{\Delta^2 - \tilde{m}^2}} \right] \\
& \left. - \int_0^1 dx \frac{32}{3} g_{\pi N \Delta}^2 \Delta \left[\sqrt{\Delta^2 - m_\pi^2} \log R - \sqrt{\Delta^2 - \tilde{m}^2} \log R[\tilde{m}^2] \right] \right\} , \quad (29)
\end{aligned}$$

$$F_2^v(q^2) = \kappa_v \left\{ 1 - \frac{g_A^2}{\kappa_v} \frac{4\pi M_N}{(4\pi F_\pi)^2} \int_0^1 dx \left[\sqrt{\tilde{m}^2} - m_\pi \right] \right. \\ \left. + \frac{32g_{\pi N\Delta}^2 M_N \Delta}{9\kappa_v (4\pi F_\pi)^2} \int_0^1 dx \left[\frac{1}{2} \log \left[\frac{\tilde{m}^2}{4\Delta^2} \right] - \log \left[\frac{m_\pi}{2\Delta} \right] \right. \right. \\ \left. \left. + \frac{\sqrt{\Delta^2 - \tilde{m}^2}}{\Delta} \log R[\tilde{m}^2] - \frac{\sqrt{\Delta^2 - m_\pi^2}}{\Delta} \log R \right] \right\}. \quad (30)$$

To obtain a better understanding of the low energy structure of the nucleon as seen by electroweak probes, it is instructive to analyse the moments of the form factors with respect to q^2 :

$$F_i^v(q^2) = F_i^v(0) \left[1 + \frac{1}{6} (r_i^v)^2 q^2 + \mathcal{O}(q^4) \right]. \quad (31)$$

The corresponding (squared) radii follow as

$$(r_1^v)^2 = 6 \frac{dF_1^v(q^2)}{dq^2} \Big|_{q^2=0} \\ = -\frac{1}{(4\pi F_\pi)^2} \left\{ 1 + 7g_A^2 + (10g_A^2 + 2) \log \left[\frac{m_\pi}{\lambda} \right] \right\} - \frac{12B_{10}^{(r)}(\lambda)}{(4\pi F_\pi)^2} \\ + \frac{g_{\pi N\Delta}^2}{54\pi^2 F_\pi^2} \left\{ 26 + 30 \log \left[\frac{m_\pi}{\lambda} \right] + 30 \frac{\Delta}{\sqrt{\Delta^2 - m_\pi^2}} \log \left[\frac{\Delta}{m_\pi} + \sqrt{\frac{\Delta^2}{m_\pi^2} - 1} \right] \right\} \\ = (0.67 + 0.13) \text{ fm}^2 - \frac{12B_{10}^{(r)}(1 \text{ GeV})}{(4\pi F_\pi)^2} = 0.80 \text{ fm}^2 - \frac{12B_{10}^{(r)}(1 \text{ GeV})}{(4\pi F_\pi)^2}, \quad (32)$$

$$(r_2^v)^2 = \frac{6}{\kappa_v} \frac{dF_2^v(q^2)}{dq^2} \Big|_{q^2=0} \\ = \frac{g_A^2 M_N}{8F_\pi^2 \kappa_v \pi m_\pi} + \frac{g_{\pi N\Delta}^2 M_N}{9F_\pi^2 \kappa_v \pi^2 \sqrt{\Delta^2 - m_\pi^2}} \log \left[\frac{\Delta}{m_\pi} + \sqrt{\frac{\Delta^2}{m_\pi^2} - 1} \right] \\ = (0.52 + 0.09) \text{ fm}^2 = 0.61 \text{ fm}^2, \quad (33)$$

Consider now the isovector Dirac radius. As it is well-known, it diverges logarithmically in the chiral limit [26]. The most precise empirical value is $(r_1^v)^2 = 0.585 \text{ fm}^2$ [27]. Already the pion loop contribution slightly overshoots this value, the $\Delta - \pi$ loop adds positively to this using the renormalization scale of $\lambda = 1 \text{ GeV}$. In that case, we have to set $B_{10}^{(r)}(1 \text{ GeV}) = 0.63$ to reproduce the empirical value of $(r_1^v)^2$. This number is of “natural size” since we expect the LECs to be of order one in units of $1/16\pi^2 F_\pi^2$.⁵ At present, we do not have a clear picture of the physics underlying $B_{10}^{(r)}$ that effectively shrinks the size of the pion-cloud in the Dirac form factor. In a “resonance-saturation” model one would expect the ρ vector meson to play a large role in $B_{10}^{(r)}$. We also note that the strength of the finite part of this counterterm can be brought to zero by reducing the value of the renormalization scale λ to 406 (858) MeV for the small scale (chiral) expansion and simultaneously reproducing the empirical value of $(r_1^v)^2$. Clearly more analysis is needed before the anatomy of this counterterm is understood.

Much easier to interpret is the isovector Pauli radius since to order ϵ^3 , it is free of any LEC. Interestingly, the novel contribution from the $\Delta - \pi$ loop leads to an increase of about 17% and brings the prediction closer to the empirical value, $(r_2^v)^2 = 0.80 \text{ fm}^2$. In the chiral limit, we recover the well known $1/m_\pi$ singularity [26]. In accord with the decoupling theorem [20], this singularity is not touched by the resonance contributions, i.e. the delta contribution vanishes for $\Delta \rightarrow \infty$.⁶

⁵To be precise, order one means any number between 0.1 and 10. This range can be taken from the presently available determinations of LECs in the nucleon sector.

⁶It is amusing to note that for the special choice $\lambda = 2\Delta$ the leading delta contribution also decouples for r_1^v . The relevance of this observation is, however, not yet clear.

In Fig.2, we show the q^2 -dependence of the isovector form factors in comparison to dispersion-theoretical result of [27]. $F_1(q^2)$ is identical in the chiral and the small scale expansion nicely reproducing the dispersion-theoretical result. For $F_2(q^2)$, the q^2 -dependence is better reproduced in the small scale than in the chiral expansion although the radius is still underestimated by about 15%. This good description of the isovector form factors is related to the two-pion continuum, whose essential features on the left wing of the ρ -resonance are reproduced in the one loop approximation. This is discussed in detail in [7]. In that paper, the chiral expansion of the spectral functions was worked out to $\mathcal{O}(p^4)$ for the isovector form factors and $\Delta(1232)$ effects were subsumed in the LEC c_4 . Finally, we compare the $\mathcal{O}(\epsilon^3)$ predictions for $F_1^v(q^2)$, $F_2^v(q^2)$ of the “small scale expansion” with the corresponding ones of $\mathcal{O}(p^3)$ HBChPT. Switching off the delta degrees of freedom via $g_{\pi N\Delta} \rightarrow 0$, the chiral prediction for $F_1^v(q^2)$ is identical to the one shown in Fig. 2, after readjusting the LEC B_{10} to give the proper radius. The resulting chiral prediction for $F_2^v(q^2)$ turns out to be worse than its “small scale expansion” analogue to this order (cf. the dot-dashed lines in Fig.2), mostly due to the known underestimation of $(r_2^v)^2$ in HBChPT at $\mathcal{O}(p^3)$. Having discussed the isovector form factors of the nucleon we now move on to the parallel discussion of the isoscalar form factors.

IV. ISOSCALAR VECTOR FORM FACTORS

A. Definition

In analogy to the isovector form factors one finds the Breit-frame reduction of the isoscalar form factors:

$$\langle N(p_2) | V_\mu^s(0) | N(p_1) \rangle = \frac{1}{N_1 N_2} \bar{u}(r_2) \left[\tilde{G}_E^s(q^2) v_\mu + \frac{1}{M_N} \tilde{G}_M^s(q^2) [S_\mu, S_\nu] q^\nu \right] u(r_1) \times \eta^\dagger \frac{1}{2} \eta \quad (34)$$

We note here that the spectral functions of the isoscalar form factors start at the three pion threshold and we thus can only have polynomial terms at one loop order (compare e.g. [7] for a more detailed discussion). Again, for the choice $v_\mu = (1, \vec{0})$, the $\tilde{G}_{E,M}^s$ correspond to the Sachs form factors $G_{E,M}^s$.

B. Chiral Input

The pertinent terms of the third order Lagrangian read:

$$\begin{aligned} \mathcal{L}_{\pi N}^{(3)} = & \frac{1}{(4\pi F_\pi)^2} \bar{N} \left\{ \tilde{B}_1 D^\mu v_{\mu\nu}^{(s)} v^\nu + B_{20} (\text{Tr}(\chi_+) i v \cdot D + \text{h.c.}) + B_{29} \Delta i [S^\mu, S^\nu] v_{\mu\nu}^s + B_{30} \Delta^2 i v \cdot D \right\} N \\ & + \frac{1}{2M_0} \bar{N} \left(\gamma_0 B_N^{(2)\dagger} \gamma_0 B_N^{(1)} + \gamma_0 B_N^{(1)\dagger} \gamma_0 B_N^{(2)} \right) N - \frac{1}{(2M_0)^2} \bar{N} \gamma_0 B_N^{(1)\dagger} \gamma_0 (i v \cdot D + \not{A} S \cdot u) B_N^{(1)} N. \end{aligned} \quad (35)$$

Here, \tilde{B}_1, B_{29} are *finite* $\mathcal{O}(\epsilon^3)$ counterterms for the reasons discussed above. In fact, B_{29} gives in principle a novel contribution to the isoscalar anomalous magnetic moment, $\kappa_s = -0.12$. However, using again the decoupling argument, its contribution has no physical consequence for the reason discussed before, see also Table 2. As in the case of the isovector form factors, we have a contribution from the nucleon Z factor encoded in the LECs B_{20} and B_{30} . Likewise, the pertinent matrices $B_N^{(i)}$ are discussed in refs. [6,13].

C. Results

In addition to the Born terms only diagrams 1b and 1f contribute to the isoscalar vector form factors. We find

$$G_E^s(q^2) = 1 + \kappa_s \frac{q^2}{4M_N^2} - 4\tilde{B}_1 \frac{q^2}{(4\pi F_\pi)^2}, \quad (36)$$

$$G_M^s(q^2) = 1 + \kappa_s, \quad (37)$$

with κ_s given in Table 2. This leads to the Dirac and Pauli form factors

$$F_1^s(q^2) = 1 - 4\tilde{B}_1 \frac{q^2}{(4\pi F_\pi)^2}, \quad (38)$$

$$F_2^s(q^2) = \kappa_s. \quad (39)$$

The LEC \tilde{B}_1 can be determined from the empirical value of $(r_1^s)^2 = (0.782 \text{ fm})^2$, $\tilde{B}_1 = -0.88$. It is again of “natural size”. The physics underlying this counterterm has not been analysed yet in a systematic fashion, but from general phenomenological and symmetry considerations we expect that a large part of the finite value of this counterterm is related to the coupling of the ω (and ϕ) vector meson to the nucleon. All of the q^2 -dependence of the isoscalar magnetic form factor and that of the isoscalar electric form factor beyond the radius is therefore given by physics which is not accessible in a $\mathcal{O}(\epsilon^3)$ calculation, to be more precise, in a one-loop calculation. The corresponding spectral functions have a cut starting at $t_0 = (3m_\pi)^2$ and thus only give non-polynomial terms at two loop order (and higher).

D. Results for the Sachs form factors

From the isoscalar and isovector components, we can reconstruct the proton and the neutron Sachs form factors,

$$G_{E,M}^p(q^2) = \frac{1}{2} (G_{E,M}^s(q^2) + G_{E,M}^v(q^2)) \quad , \quad G_{E,M}^n(q^2) = \frac{1}{2} (G_{E,M}^s(q^2) - G_{E,M}^v(q^2)) \quad . \quad (40)$$

In Fig. 3a, the resulting proton form factors are shown in comparison to the dispersion-theoretical result [27] and the dipole fit

$$G_E^p(q^2) = G_M^p(q^2)/\mu_p = G_M^n(q^2)/\mu_n = (1 - q^2/0.71 \text{ GeV}^2)^{-2} \quad , \quad (41)$$

with $\mu_{p,n}$ the magnetic moment of the proton and the neutron, respectively. The corresponding neutron form factors are shown in Fig. 3b. We note that since the isoscalar magnetic form factor is a constant to this order, the q^2 -dependence of G_M^p and G_M^n is identical. This also holds for the chiral expansion to order p^3 . The three form factors $G_{E,M}^p$, G_M^n are rather well described by the ϵ^3 results for momenta squared smaller than 0.2 GeV^2 . The electric form factor $G_E^n(q^2)$ of the neutron is much smaller in magnitude than the other three form factors of the nucleon (therefore, it is amplified in the figure by a factor of ten). The slope of $G_E^n(q^2)$ is related to the “electric radius” of the neutron via

$$\begin{aligned} (r_E^n)^2 &= 6 \frac{d G_E^n(q^2)}{dq^2} \Big|_{q^2=0} \\ &= 6 \left[\frac{d F_1^n(q^2)}{dq^2} + \frac{\kappa_n}{4M_N^2} \right] \\ &= -0.113 \text{ fm}^2 \quad , \end{aligned} \quad (42)$$

which is nearly completely dominated by the contribution from the anomalous magnetic moment (Foldy-term). The q^2 -dependence of G_E^n is reasonably well described up to momenta squared of about 0.1 GeV^2 . Note that the smallness of this form factor stems from a cancellation of too large contributions (isovector versus isoscalar currents) and thus small inaccuracies in describing either one of these show up visibly in G_E^n .

V. AXIAL FORM FACTORS

In addition to the electromagnetic form factors, the axial ones give further information about the structure of the nucleon. In particular, the axial current is only partially conserved and the axial charge is not equal to one. These facts are, of course, at the heart of the chiral symmetry approach to the nucleon structure.

A. Definition

In the absence of second class currents, i.e. currents which have opposite G-parity to the ones defined by the operators $\gamma_\mu \gamma_5$ and $q_\mu \gamma_5$,⁷ the most general matrix element of the isovector axial current operator which conserves parity and time reversal invariance is

⁷Experimentally, such second class currents are excluded to a high precision.

$$\langle N(p_2)|A_\mu^i(0)|N(p_1)\rangle = \bar{u}(p_2) \left[G_A(q^2) \gamma_\mu \gamma_5 + \frac{1}{2M_N} G_P(q^2) q_\mu \gamma_5 \right] u(p_1) \times \eta^\dagger \frac{\tau^i}{2} \eta . \quad (43)$$

Here, $G_A(q^2)$ and $G_P(q^2)$ are the axial and the induced pseudoscalar form factor, respectively. While $G_A(q^2)$ can be extracted from (anti)neutrino–proton scattering or charged pion electroproduction data, $G_P(q^2)$ can be determined in some kinematical range from ordinary and radiative muon capture as well as from pion electroproduction.

We perform a non-relativistic reduction of this matrix element in the Breit frame with the same kinematics used for the electromagnetic form factors. This gives

$$\langle N(p_2)|A_0^i(0)|N(p_1)\rangle = 0 \quad (44)$$

$$\langle N(p_2)|A_a^i(0)|N(p_1)\rangle = \chi_2^\dagger \left[\frac{E}{M_N} G_A(q^2) \sigma^a - \left(\frac{E - M_N}{M_N} G_A(q^2) - \frac{q^2}{4M_N^2} G_P(q^2) \right) \hat{q}^a \vec{\sigma} \cdot \hat{q} \right] \chi_1 \times \eta^\dagger \frac{\tau^i}{2} \eta , \quad (45)$$

where χ denotes the 2-component spinor of the nucleon, σ^a ($a = 1, 2, 3$) represents a Pauli matrix and \hat{q} is a unit vector in the direction of \vec{q} . The vanishing of the nucleon matrix element $\langle N(p_2)|A_0^i(0)|N(p_1)\rangle$ is equivalent to the absence of second class currents.

B. Chiral Input

First, we need some terms of the next-to-leading order meson Lagrangian. Since our πN Lagrangian is the heavy baryon version of the form used in [5], we have to use the appropriate version of $\mathcal{L}_{\pi\pi}^{(4)}$,

$$\mathcal{L}_{\pi\pi}^{(4)} = \frac{1}{16} l_3 \text{Tr}(\chi_+)^2 + \frac{1}{16} l_4 \left[2\text{Tr}(\chi_+) \text{Tr}(u \cdot u) + 2\text{Tr}(\chi_-^2) - \text{Tr}(\chi_-)^2 \right] , \quad (46)$$

with

$$l_i = l_i^r(\lambda) + \gamma_i L . \quad (47)$$

The LECs l_3 and l_4 contribute to the renormalization of the pion mass and decay constant (using $\gamma_3 = 1/2$, $\gamma_4 = -2/3$),

$$m_\pi^2 = m_0^2 + \frac{m_0^4}{F_\pi^2} \left(2l_3^r(\lambda) + \frac{1}{16\pi^2} \log \left[\frac{m_\pi}{\lambda} \right] \right) , \quad (48)$$

$$F_\pi = F_0 + \frac{m_0^2}{F_0} \left(l_4^r(\lambda) - \frac{1}{8\pi^2} \log \left[\frac{m_\pi}{\lambda} \right] \right) , \quad (49)$$

with $m_0^2 = (m_u + m_d) |\langle 0|\bar{q}q|0\rangle|/F_0^2$ the leading term in the quark mass expansion of the pion mass squared and we assume the standard scenario of dynamical chiral symmetry breaking (large condensate). F_0 is the SU(2) chiral limit value of the pion decay constant. The relevant terms involving nucleons and deltas take the form

$$\begin{aligned} \mathcal{L}_{\pi N}^{(3)} = & \frac{1}{(4\pi F_\pi)^2} \bar{N} \left\{ B_9 S \cdot u \text{Tr}(\chi_+) + \tilde{B}_2 i [S \cdot D, \chi_-] + \tilde{B}_3 S^\mu [D^\nu, f_{\mu\nu}^-] \right\} N \\ & - \frac{1}{(2M_0)^2} \bar{N} \gamma_0 B_N^{(1)\dagger} \gamma_0 (iv \cdot D + \dot{g}_A S \cdot u) B_N^{(1)} N . \end{aligned} \quad (50)$$

\tilde{B}_2, \tilde{B}_3 are finite counterterms. Their meaning is discussed in the next sections. In addition, the fixed $1/M^2$ contributions are solely governed by the matrix $B_N^{(1)}$, which can be found in refs. [6,13].

C. Results

The chiral calculation yields results in the form

$$\langle N(p_2)|A_0^i(0)|N(p_1)\rangle = 0 , \quad (51)$$

$$\langle N(p_2)|A_a^i(0)|N(p_1)\rangle = \chi_2^\dagger \left[G_1(q^2) \sigma^a + G_2(q^2) \hat{q}^a \vec{\sigma} \cdot \hat{q} \right] \chi_1 \times \eta^\dagger \frac{\tau^i}{2} \eta . \quad (52)$$

Adding the loop amplitudes of Appendix B to the Born and counterterm contributions one finds in the Breit frame

$$G_1^{(3)}(q^2) = g_A - \frac{q^2}{8M_N^2} g_A + \frac{q^2}{(4\pi F_\pi)^2} \tilde{B}_3, \quad (53)$$

$$G_2^{(3)}(q^2) = \frac{q^2}{8M_N^2} g_A - g_A \frac{q^2}{q^2 - m_\pi^2} + \frac{2m_\pi^2 \tilde{B}_2}{(4\pi F_\pi)^2} \frac{q^2}{q^2 - m_\pi^2} - \tilde{B}_3 \frac{q^2}{(4\pi F_\pi)^2}. \quad (54)$$

The rather lengthy renormalization of g_A is given in Table 2. However, these are not the quantities one is usually interested in. The connection between $G_1(q^2), G_2(q^2)$ and the relativistic axial form factors $G_A(q^2), G_P(q^2)$ to $\mathcal{O}(\epsilon^3)$ in the small scale expansion reads

$$G_1(q^2) = G_A(q^2) - \frac{q^2}{8M_N^2} g_A + \mathcal{O}(1/M_N^3), \quad (55)$$

$$G_2(q^2) = \frac{q^2}{8M_N^2} g_A + \frac{q^2}{4M_N^2} G_P(q^2) + \mathcal{O}(1/M_N^3), \quad (56)$$

yielding

$$G_A(q^2) = g_A + \frac{q^2}{(4\pi F_\pi)^2} \tilde{B}_3, \quad (57)$$

$$G_P(q^2) = \frac{4M_N^2}{m_\pi^2 - q^2} \left[g_A - \frac{2m_\pi^2 \tilde{B}_2}{(4\pi F_\pi)^2} \right] - \tilde{B}_3 \frac{4M_N^2}{(4\pi F_\pi)^2}. \quad (58)$$

The meaning of the finite shift governed by \tilde{B}_2 together with the induced pseudoscalar form factor G_P will be discussed in the following section, whereas the finite counterterm \tilde{B}_3 has the simple interpretation as the radius of the axial form factor:

$$\begin{aligned} (r_A)^2 &= \frac{6}{g_A} \left. \frac{d G_A(q^2)}{dq^2} \right|_{q^2=0} \\ &= \frac{\tilde{B}_3}{g_A} \frac{6}{(4\pi F_\pi)^2} \equiv (0.65 \pm 0.03)^2 \text{ fm}^2, \end{aligned} \quad (59)$$

using the mean value of the axial radius deduced from (anti)neutrino–proton scattering.⁸ This gives $\tilde{B}_3 = 3.08 \pm 0.27$. Although we have fixed the numerical strength of this counterterm, more analysis is needed to understand the physics underlying \tilde{B}_3 . Presumably one will find an interplay between axial-vector meson a_1 and ρ – π continuum contributions. Furthermore, as in the case of the isoscalar electromagnetic form factor, the pertinent axial spectral function starts with the three-pion cut. Therefore, a one loop calculation can only lead to polynomial contributions to the axial form factors. The small momentum behavior of the axial spectral function in the framework of HBChPT is discussed in [7]. We note that $\Delta(1232)$ effects only appear in the renormalization of the axial–vector coupling constant (cf. Table 2) but not in the axial radius, yielding exactly the same result for this form factor as in the chiral $\mathcal{O}(p^3)$ calculations [6,10], once the different coupling constant renormalizations have been taken into account.

VI. ELECTROWEAK FORM FACTORS AND MUON CAPTURE

Here, we wish to discuss the induced pseudoscalar form factor and the corresponding coupling g_P [9,10,28]. It is defined as the form factor for the kinematics of ordinary muon capture on the proton (at rest),

$$g_P \equiv \frac{m_\mu}{2M_N} G_P(q^2 = -0.88m_\mu^2)$$

⁸Here, we do not consider the axial radius extracted from charged pion electroproduction since a systematic analysis of such processes in the small scale expansion is not yet available.

$$\begin{aligned}
&= \frac{2m_\mu}{m_\pi^2 + 0.88m_\mu^2} g_A M_N \left[1 - \frac{2m_\pi^2 \tilde{B}_2}{(4\pi F_\pi)^2 g_A} \right] - \frac{1}{3} g_A m_\mu M_N r_A^2 \\
&= \frac{2m_\mu F_\pi g_{\pi NN}}{m_\pi^2 + 0.88m_\mu^2} - \frac{1}{3} g_A m_\mu M_N r_A^2 \\
&= 8.46 \text{ (8.23)} ,
\end{aligned} \tag{60}$$

for $m_\mu = 0.106 \text{ GeV}$, $g_{\pi NN} = 13.4 \text{ (13.05)}$ and we have made use of Eq.(59) and of the definition of the Goldberger-Treiman deviation

$$\Delta_{\text{GT}} \equiv 1 - \frac{g_A M_N}{F_\pi g_{\pi NN}} = -\frac{m_\pi^2 \tilde{B}_2}{8\pi^2 F_\pi^2 g_A} \ll 1 . \tag{61}$$

The precise value of Δ_{GT} depends on the values one chooses for g_A and $g_{\pi NN}$. In Table 3, taken from [28], we have collected the most recent ranges allowed by various input data.⁹ We note that as in the case of $G_A(q^2)$, Eq.(60), obtained in the small scale expansion including the $\Delta(1232)$, agrees exactly with the chiral prediction (obtained in HBChPT) to order p^3 . In fact, this remarkable prediction for g_P agrees also with the pre-QCD analysis of Adler and Dothan [29] [30] and is extremely precise [9].

Accordingly, to third order both in HBChPT and in the small scale expansion the pseudoscalar form factor of the nucleon can be expressed as

$$G_P^{(3)}(q^2) = \frac{4M_N g_{\pi NN} F_\pi}{m_\pi^2 - q^2} - \frac{2}{3} g_A M_N^2 r_A^2 , \tag{62}$$

which modifies the by now outdated pion pole (i.e. $\mathcal{O}(\epsilon^2)$) prediction

$$G_P^{(2)}(q^2) = \frac{4M_N g_{\pi NN} F_\pi}{m_\pi^2 - q^2} . \tag{63}$$

Apart from the pion pole, one needs three-pion intermediate states to build up additional non-polynomial dependence in $G_P(q^2)$ in the small scale as well as the chiral expansion (i.e. one has to go to two loops). So far, the only experiment in which the induced pseudoscalar form factor was extracted in a certain kinematical range was the pion electroproduction one at Saclay [31] (see also [32] for some comments). Within the precision of the experiment, the q^2 -dependence induced by the pion pole could be verified. More precise data are certainly needed to further test the chiral/small scale prediction for $G_P(q^2)$. Finally, we note that the recently published TRIUMF radiative muon capture experiment [14] finds a very large value for the induced pseudoscalar coupling constant, $g_P^{\text{Triumf}} = (9.8 \pm 0.7 \pm 0.3) g_A$. This is about 50% larger than the prediction in the chiral or small scale expansion. It is not yet clear whether this result has to be considered genuine or needs, e.g., to be subjected to further radiative (or other) corrections, see e.g. [10] [33] [34] [35]. From our calculation we must conclude that to this order $\Delta(1232)$ effects in the electroweak form factors can not explain the TRIUMF number.

VII. ACKNOWLEDGMENTS

We would like to acknowledge helpful discussions with our colleague Hans-Werner Hammer. This work was supported in part by the Natural Sciences and Engineering Research Council of Canada.

⁹Also given in that table is the value of the monopole cut-off of the pion-nucleon vertex function, which can be extracted from the Goldberger-Treiman discrepancy under the assumption that it is entirely due to the strong πN form factor.

APPENDIX A: LOOP DIAGRAMS OF THE VECTOR FORM FACTORS

There are six non-zero loop diagrams (cf. Fig.1) at $\mathcal{O}(\epsilon^3)$ contributing to the vector form factors. One finds

$$A_{1a} = i \frac{g_A^2}{(4\pi F_\pi)^2} \eta^\dagger \frac{\tau^i}{2} \eta \left\{ \bar{u}(r_2) \epsilon_v \cdot v u(r_1) \left[\left(6m_\pi^2 - \frac{5}{3}q^2 \right) \left(16\pi^2 L + \log \frac{m_\pi}{\lambda} \right) + 2m_\pi^2 - \frac{2}{3}q^2 \right. \right. \\ \left. \left. + \int_0^1 dx \left(3m_\pi^2 - 5q^2 x(1-x) \right) \log \left[\frac{\tilde{m}^2}{m_\pi^2} \right] \right] \right. \\ \left. - \bar{u}(r_2) [S_\mu, S_\nu] \epsilon_v^\mu q^\nu u(r_1) \int_0^1 dx 4\pi \sqrt{\tilde{m}^2} \right\} \quad (A1)$$

$$A_{1b} = i \frac{g_A^2}{(4\pi F_\pi)^2} \left\{ \eta^\dagger \frac{1}{2} \eta \bar{u}(r_2) \epsilon_v \cdot v u(r_1) \left[\frac{3}{2}m_\pi^2 + \frac{9}{2}m_\pi^2 \left(16\pi^2 L + \log \frac{m_\pi}{\lambda} \right) \right] \right. \\ \left. - \eta^\dagger \frac{\tau^i}{2} \eta \bar{u}(r_2) \epsilon_v \cdot v u(r_1) \left[\frac{m_\pi^2}{2} + \frac{3}{2}m_\pi^2 \left(16\pi^2 L + \log \frac{m_\pi}{\lambda} \right) \right] \right\} \quad (A2)$$

$$A_{1c} = i \frac{-1}{(4\pi F_\pi)^2} \eta^\dagger \frac{\tau^i}{2} \eta \bar{u}(r_2) \epsilon_v \cdot v u(r_1) \left\{ 2m_\pi^2 \left(16\pi^2 L + \log \frac{m_\pi}{\lambda} \right) \right\} \quad (A3)$$

$$A_{1d} = i \frac{1}{(4\pi F_\pi)^2} \eta^\dagger \frac{\tau^i}{2} \eta \bar{u}(r_2) \epsilon_v \cdot v u(r_1) \left\{ \left(2m_\pi^2 - \frac{1}{3}q^2 \right) \left(16\pi^2 L + \log \frac{m_\pi}{\lambda} \right) + \int_0^1 dx \tilde{m}^2 \log \frac{\tilde{m}^2}{m_\pi^2} \right\} \quad (A4)$$

$$A_{1e} = i \frac{8g_{\pi N\Delta}^2}{(4\pi F_\pi)^2} \eta^\dagger \frac{\tau^i}{2} \eta \left\{ \bar{u}(r_2) \epsilon_v \cdot v u(r_1) \left[\left(\frac{2}{3}(2\Delta^2 - m_\pi^2) + \frac{5}{27}q^2 \right) \left(16\pi^2 L + \log \frac{m_\pi}{\lambda} \right) - \frac{1}{3}m_\pi^2 + \frac{17}{162}q^2 \right. \right. \\ \left. \left. + \int_0^1 dx \frac{1}{3} \left(2\Delta^2 - m_\pi^2 + \frac{5}{3}q^2 x(1-x) \right) \log \frac{\tilde{m}^2}{m_\pi^2} \right. \right. \\ \left. \left. + \int_0^1 dx \frac{1}{3} \left(\frac{4}{3}q^2 x(1-x) \frac{\Delta}{\sqrt{\Delta^2 - \tilde{m}^2}} + 4\Delta \sqrt{\Delta^2 - \tilde{m}^2} \right) \log R[\tilde{m}^2] \right] \right. \\ \left. + \bar{u}(r_2) [S_\mu, S_\nu] \epsilon_v^\mu q^\nu u(r_1) \left[\frac{4}{9}\Delta \left(16\pi^2 L + \log \frac{m_\pi}{\lambda} \right) - \frac{10}{27}\Delta \right. \right. \\ \left. \left. + \int_0^1 dx \left(\frac{2}{9}\Delta \log \left[\frac{\tilde{m}^2}{m_\pi^2} \right] + \frac{4}{9}\sqrt{\Delta^2 - \tilde{m}^2} \log R[\tilde{m}^2] \right) \right] \right\} \quad (A5)$$

$$A_{1f} = i \frac{-8g_{\pi N\Delta}^2}{(4\pi F_\pi)^2} \left\{ \eta^\dagger \frac{1}{2} \eta \bar{u}(r_2) \epsilon_v \cdot v u(r_1) \left[(2\Delta^2 - m_\pi^2) \left(16\pi^2 L + \log \frac{m_\pi}{\lambda} \right) - \frac{m_\pi^2}{2} + 2\Delta \sqrt{\Delta^2 - m_\pi^2} \log R[m_\pi^2] \right] \right. \\ \left. + \eta^\dagger \frac{\tau^i}{2} \eta \bar{u}(r_2) \epsilon_v \cdot v u(r_1) \left[\frac{5}{3}(2\Delta^2 - m_\pi^2) \left(16\pi^2 L + \log \frac{m_\pi}{\lambda} \right) - \frac{5}{6}m_\pi^2 \right. \right. \\ \left. \left. + \frac{10}{3}\Delta \sqrt{\Delta^2 - m_\pi^2} \log R[m_\pi^2] \right] \right\}, \quad (A6)$$

with $\tilde{m}^2 = m_\pi^2 - q^2 x(1-x)$ and $R[z] = \frac{\Delta}{\sqrt{z}} + \sqrt{\frac{\Delta^2}{z^2} - 1}$.

APPENDIX B: LOOP DIAGRAMS OF THE AXIAL FORM FACTORS

There are 12 non-zero loop diagrams (cf. Fig.4) at $\mathcal{O}(\epsilon^3)$ contributing to the axial form factors. One finds

$$A_{2a} = i \frac{g_A}{(4\pi F_\pi)^2} \eta^\dagger \frac{\tau^i}{2} \eta \bar{u}(r_2) \frac{S \cdot q \epsilon_a \cdot q}{q^2 - m_\pi^2} u(r_1) 2m_\pi^2 \left(16\pi^2 L + \log \frac{m_\pi}{\lambda} \right) \quad (B1)$$

$$A_{2b} = i \frac{g_A}{(4\pi F_\pi)^2} \eta^\dagger \frac{\tau^i}{2} \eta \bar{u}(r_2) \frac{S \cdot q \epsilon_a \cdot q}{q^2 - m_\pi^2} u(r_1) \left(16\pi^2 L + \log \frac{m_\pi}{\lambda} \right) \frac{4m_\pi^2 q^2 - 6m_\pi^4}{q^2 - m_\pi^2} \quad (B2)$$

$$A_{2c} = i \frac{-g_A}{(4\pi F_\pi)^2} \eta^\dagger \frac{\tau^i}{2} \eta \bar{u}(r_2) \frac{S \cdot q \epsilon_a \cdot q}{q^2 - m_\pi^2} u(r_1) 2m_\pi^2 \left(16\pi^2 L + \log \frac{m_\pi}{\lambda} \right) \quad (B3)$$

$$A_{2d} = i \frac{-g_A}{(4\pi F_\pi)^2} \eta^\dagger \frac{\tau^i}{2} \eta \bar{u}(r_2) S \cdot \epsilon_a u(r_1) 4m_\pi^2 \left(16\pi^2 L + \log \frac{m_\pi}{\lambda} \right) \quad (B4)$$

$$A_{2e} = i \frac{g_A^3}{(4\pi F_\pi)^2} \eta^\dagger \frac{\tau^i}{2} \eta \bar{u}(r_2) S \cdot \epsilon_a u(r_1) m_\pi^2 \left(16\pi^2 L + \log \frac{m_\pi}{\lambda} + 1 \right) \quad (B5)$$

$$A_{2f} = i \frac{-g_A^3}{(4\pi F_\pi)^2} \eta^\dagger \frac{\tau^i}{2} \eta \bar{u}(r_2) \frac{S \cdot q \epsilon_a \cdot q}{q^2 - m_\pi^2} u(r_1) m_\pi^2 \left(16\pi^2 L + \log \frac{m_\pi}{\lambda} + 1 \right) \quad (B6)$$

$$A_{2g} = i \frac{g_A g_{\pi N \Delta}^2}{(4\pi F_\pi)^2} \eta^\dagger \frac{\tau^i}{2} \eta \bar{u}(r_2) S \cdot \epsilon_a u(r_1) \frac{32}{9} \left\{ \left(2m_\pi^2 - \frac{4}{3} \Delta^2 \right) \left(16\pi^2 L + \log \frac{m_\pi}{\lambda} \right) + \frac{8}{9} \Delta^2 - m_\pi^2 \right. \\ \left. + \frac{2}{3} \frac{\pi m_\pi^3}{\Delta} - \frac{4}{3} \frac{(\Delta^2 - m_\pi^2)^{3/2}}{\Delta} \log R[m_\pi^2] \right\} \quad (B7)$$

$$A_{2h} = A_{2g} \quad (B8)$$

$$A_{2i} = i \frac{g_1 g_{\pi N \Delta}^2}{(4\pi F_\pi)^2} \eta^\dagger \frac{\tau^i}{2} \eta \bar{u}(r_2) S \cdot \epsilon_a u(r_1) \frac{400}{81} \left\{ (2\Delta^2 - m_\pi^2) \left(16\pi^2 L + \log \frac{m_\pi}{\lambda} \right) + \Delta^2 - m_\pi^2 + \frac{2\Delta^2 - m_\pi^2}{30} \right. \\ \left. + 2\Delta \sqrt{\Delta^2 - m_\pi^2} \log R[m_\pi^2] \right\} \quad (B9)$$

$$A_{2j} = i \frac{-g_A g_{\pi N \Delta}^2}{(4\pi F_\pi)^2} \eta^\dagger \frac{\tau^i}{2} \eta \bar{u}(r_2) \frac{S \cdot q \epsilon_a \cdot q}{q^2 - m_\pi^2} u(r_1) \frac{32}{9} \left\{ \left(2m_\pi^2 - \frac{4}{3} \Delta^2 \right) \left(16\pi^2 L + \log \frac{m_\pi}{\lambda} \right) + \frac{8}{9} \Delta^2 - m_\pi^2 \right. \\ \left. + \frac{2}{3} \frac{\pi m_\pi^3}{\Delta} - \frac{4}{3} \frac{(\Delta^2 - m_\pi^2)^{3/2}}{\Delta} \log R[m_\pi^2] \right\} \quad (B10)$$

$$A_{2k} = A_{2j} \quad (B11)$$

$$A_{2l} = i \frac{-g_1 g_{\pi N \Delta}^2}{(4\pi F_\pi)^2} \eta^\dagger \frac{\tau^i}{2} \eta \bar{u}(r_2) \frac{S \cdot q \epsilon_a \cdot q}{q^2 - m_\pi^2} u(r_1) \frac{400}{81} \left\{ (2\Delta^2 - m_\pi^2) \left(16\pi^2 L + \log \frac{m_\pi}{\lambda} \right) + \Delta^2 - m_\pi^2 + \frac{2\Delta^2 - m_\pi^2}{30} \right. \\ \left. + 2\Delta \sqrt{\Delta^2 - m_\pi^2} \log R[m_\pi^2] \right\} \quad (B12)$$

- [1] Ulf-G. Meißner, Phys. Rep. 161, 213 (1988)
- [2] F. Klein and H. Schmieden, Nucl. Phys. A623, 323c (1997)
- [3] Ulf-G. Meißner, Nucl. Phys. A623, 340c (1997)
- [4] D. Drechsel et al., [nucl-th/9712013]
- [5] J. Gasser, M.E. Sainio, and A. Svarc, Nucl. Phys. B307, 779 (1988)
- [6] V. Bernard, J. Kambor, N. Kaiser, and Ulf-G. Meißner, Nucl. Phys. B388, 315 (1992)
- [7] V. Bernard, N. Kaiser, and Ulf-G. Meißner, Nucl. Phys. A611, 429 (1996)
- [8] V. Bernard, N. Kaiser, and Ulf-G. Meißner, Phys. Rev. Lett. 69, 1877 (1992)
- [9] V. Bernard, N. Kaiser, and Ulf-G. Meißner, Phys. Rev. D50, 6899 (1994)
- [10] H.W. Fearing, R. Lewis, N. Mobed, and S. Scherer, Phys. Rev. D56, 1783 (1997)
- [11] E. Jenkins and A.V. Manohar, Phys. Lett. B259, 353 (1991)
- [12] T.R. Hemmert, B.R. Holstein, and J. Kambor, Phys. Lett. B395, 89 (1997)
- [13] T.R. Hemmert, B.R. Holstein, and J. Kambor, [hep/ph-9712496] and "Chiral Lagrangians and Δ Interactions: Applications", in preparation
- [14] G. Jonkmans et al., Phys. Rev. Lett. 77, 4512 (1996)
- [15] D. S. Beder and H. W. Fearing, Phys. Rev. D35, 2130 (1987); *ibid.* D39, 3493 (1989).
- [16] V. Bernard, N. Kaiser, and Ulf-G. Meißner, Nucl. Phys. A615, 483 (1997)
- [17] V. Bernard, N. Kaiser, and Ulf-G. Meißner, Int. J. Mod. Phys. E4, 193 (1995)
- [18] G. Ecker, Phys. Lett. B336, 508 (1994)
- [19] N. Fettes, Ulf-G. Meißner and S. Steininger, preprint FZJ-IKP(TH)-1998-03
- [20] J. Gasser and A. Zepeda, Nucl. Phys. B174, 445 (1980)

- [21] Ulf-G. Meißner, in *N* Physics*, ed. by T.-S.H. Lee and W. Roberts (World Scientific, Singapore, 1997), p. 90
- [22] V. Bernard, N. Kaiser, and Ulf-G. Meißner, Z. Phys. C60, 111 (1993)
- [23] J. Kambor, [hep-ph/9711484]
- [24] G. Ecker and M. Mojžiš, Phys. Lett. B410, 266 (1997)
- [25] G. Ecker and M. Mojžiš, Phys. Lett. B365, 312 (1996)
- [26] M.A.B. Bég and A. Zepeda, Phys. Rev. D6, 2912 (1972)
- [27] P. Mergell, Ulf-G. Meißner, and D. Drechsel, Nucl. Phys. A596, 367 (1996)
- [28] Ulf-G. Meißner, [hep-ph/9711365]
- [29] S.L. Adler and Y. Dothan, Phys. Rev. 151, 1257 (1966)
- [30] L. Wolfenstein, in *High-Energy Physics and Nuclear Structure*, ed. by S. Devons (Plenum, New York, 1970), p.661
- [31] S. Choi et al., Phys. Rev. Lett. 71, 3927 (1993)
- [32] V. Bernard, N. Kaiser and Ulf-G. Meißner, Phys. Rev. Lett. 72, 2810(C) (1994)
- [33] T. Meissner, F. Myhrer, and K. Kubodera, Phys. Lett. B416, 36 (1998)
- [34] S.-I. Ando and D.-P. Min, Phys. Lett. B417, 177 (1998)
- [35] H. W. Fearing, R. Lewis, N. Mobed, and S. Scherer, Proc. of the XVth Int. Conf. on Few Body Problems in Physics, Groningen, The Netherlands, July, 1997, (in press)

Tables

LEC	O_i	β_i at $\mathcal{O}(p^3)$	β_i at $\mathcal{O}(\epsilon^3)$	phen.
B_9	$S \cdot u \text{ Tr}(\chi_+)$	$\frac{g_A}{2} - \frac{g_A^3}{8}$	$\frac{g_A}{2} - \frac{g_A^3}{8} - g_A g_{\pi N \Delta}^2 \frac{16}{9} + g_1 g_{\pi N \Delta}^2 \frac{50}{81}$	g_A
B_{10}	$(D^\mu f_{\mu\nu}^+ v^\nu)$	$-\frac{1}{6} - \frac{5}{6} g_A^2$	$-\frac{1}{6} - \frac{5}{6} g_A^2 + \frac{20}{27} g_{\pi N \Delta}^2$	$(r_1^v)^2$
B_{20}	$\text{Tr}(\chi_+) i v \cdot D + h.c.$	$-\frac{9}{16} g_A^2$	$-\frac{9}{16} g_A^2 - g_{\pi N \Delta}^2$	Z_N
B_{28}	$i [S^\mu, S^\nu] f_{\mu\nu}^+$	-	$+\frac{8}{9} g_{\pi N \Delta}^2$	κ_v
B_{29}	$i [S^\mu, S^\nu] v_{\mu\nu}^s$	-	0	κ_s
B_{30}	$i v \cdot D$	-	$+16 g_{\pi N \Delta}^2$	Z_N
B_{31}	$S \cdot u$	-	$+g_A g_{\pi N \Delta}^2 \frac{128}{27} - g_1 g_{\pi N \Delta}^2 \frac{400}{81}$	g_A

TABLE I. Comparison of the counterterm structures between HBChPT and the small scale expansion.

κ_s	=	$\dot{\kappa}_s - 4B_{29} \frac{\Delta M_N}{(4\pi F_\pi)^2}$
κ_v	=	$\dot{\kappa}_v - g_A^2 \frac{4\pi m_\pi M_N}{(4\pi F_\pi)^2} - \frac{4\Delta M_N}{(4\pi F_\pi)^2} \left[B_{28}^{(r)}(\lambda) + \frac{20}{27} g_{\pi N \Delta}^2 - \frac{8}{9} g_{\pi N \Delta}^2 \log \frac{2\Delta}{\lambda} \right] + \frac{32}{9} g_{\pi N \Delta}^2 \frac{M_N \Delta}{(4\pi F_\pi)^2} \left(\log \left[\frac{m_\pi}{2\Delta} \right] + \frac{\sqrt{\Delta^2 - m_\pi^2}}{\Delta} \log R \right)$
g_A	=	$\dot{g}_A Z_N^{(3)} + \frac{m_\pi^2}{32\pi^2 F_\pi^2} \left[8B_9^r(\lambda) + \log \left[\frac{m_\pi}{\lambda} \right] (g_A^3 - 4g_A) + g_A^3 \right] + \frac{\Delta^2}{(4\pi F_\pi)^2} B_{31}^r(\lambda)$ $+ \frac{g_A g_{\pi N \Delta}^2}{32\pi^2 F_\pi^2} \left(\frac{128}{9} m_\pi^2 - \frac{256}{27} \Delta^2 \right) \log \left[\frac{m_\pi}{\lambda} \right] + \frac{g_A g_{\pi N \Delta}^2}{32\pi^2 F_\pi^2} \left(\frac{512}{81} \Delta^2 - \frac{64}{9} m_\pi^2 + \frac{128}{27} \pi \frac{m_\pi^3}{\Delta} - \frac{256}{27} \frac{(\Delta^2 - m_\pi^2)^{3/2}}{\Delta} \log R \right)$ $+ \frac{g_1 g_{\pi N \Delta}^2}{32\pi^2 F_\pi^2} \frac{400}{81} \left\{ (2\Delta^2 - m_\pi^2) \log \left[\frac{m_\pi}{\lambda} \right] + \Delta^2 - m_\pi^2 + \frac{2\Delta^2 - m_\pi^2}{30} + 2\Delta \sqrt{\Delta^2 - m_\pi^2} \log R \right\}$

TABLE II. Renormalization of coupling constants in the small scale expansion.

g_A	F_π [MeV]	$g_{\pi N}$	Δ_{GT} [%]	\tilde{B}_2	Λ [MeV]
1.260	92.42	13.40	4.5	-1.57	656
1.260	92.42	13.05	2.0	-0.68	994
1.266	92.42	13.40	4.1	-1.41	691
1.266	92.42	13.05	1.5	-0.52	1135

TABLE III. The Goldberger–Treiman discrepancy Δ_{GT} for various input parameters, as taken from [28]. Also given are the LEC \tilde{B}_2 and the pion–nucleon cut-off as explained in the text. Note that for this table we have used more precise values of F_π and M_N than elsewhere in the main text.

Figure Captions

- Fig.1 One-loop diagrams contributing to the vector form factors. The graphs a,b,c,d are the standard graphs (chiral expansion to order p^3) whereas e and f are the new contributions in the small scale expansion at $\mathcal{O}(\epsilon^3)$. Nucleons, Δ 's, pions and photons are denoted by solid, double, dashed and wiggly lines, respectively.
- Fig.2 Small scale expansion of the isovector nucleon form factors (solid lines) in comparison to the empirical parameterization of [27] (dashed lines) and the order p^3 chiral expansion (dot-dashed lines). The lower (upper) set of curves refers to $F_1^v(q^2)$ ($F_2^v(q^2)$).
- Fig.3 (a) Proton Sachs form factors. Solid lines: Small scale expansion, dashed lines: dipole fit, dashed-dotted lines: dispersion-theoretical result [27]. The upper and the lower curves refer to $G_M^p(q^2)$ and $G_E^p(q^2)$, respectively. (b) Neutron Sachs form factors (the dipole prediction for G_E^n is zero and not shown). The upper and the lower curves refer to $G_E^n(q^2)$ and $G_M^n(q^2)$, respectively. Note that $G_E^n(q^2)$ is multiplied by a factor of ten.
- Fig.4 One-loop diagrams contributing to the axial form factors (including the ones which simply renormalize the mass, the propagator and the decay constant of the pion). The graphs a,...,f are the standard graphs whereas h,...,l are the new contributions in the small scale expansion at $\mathcal{O}(\epsilon^3)$. The circle-cross denotes the coupling to the external axial-vector source.

Figures

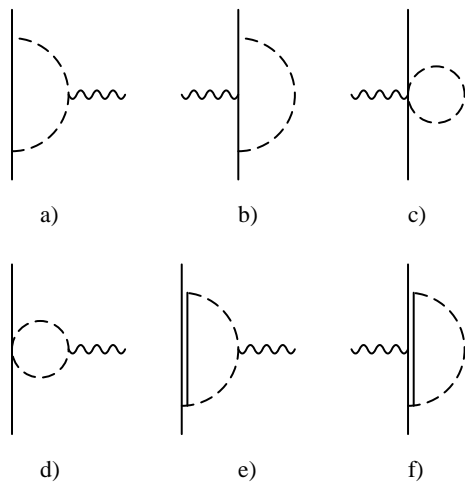


Figure 1

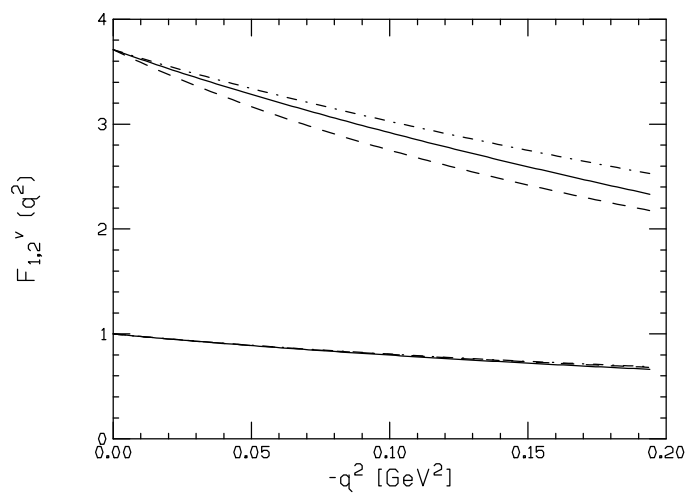


Figure 2

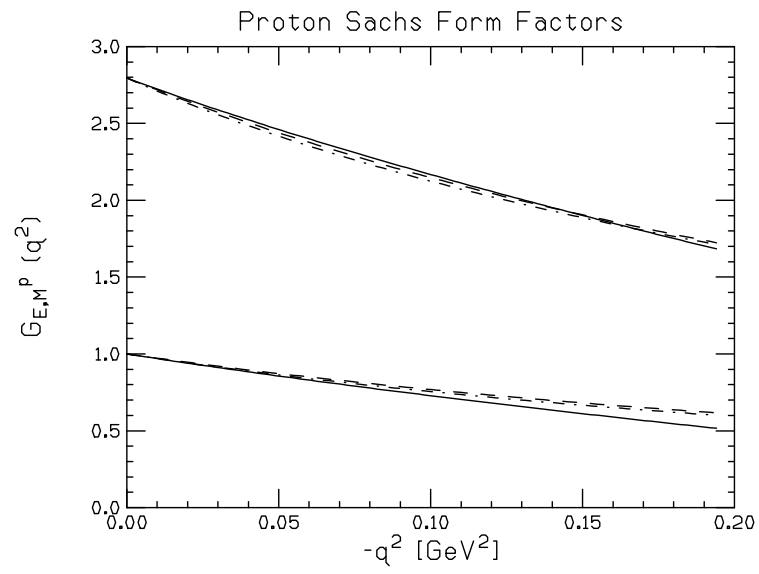


Figure 3a

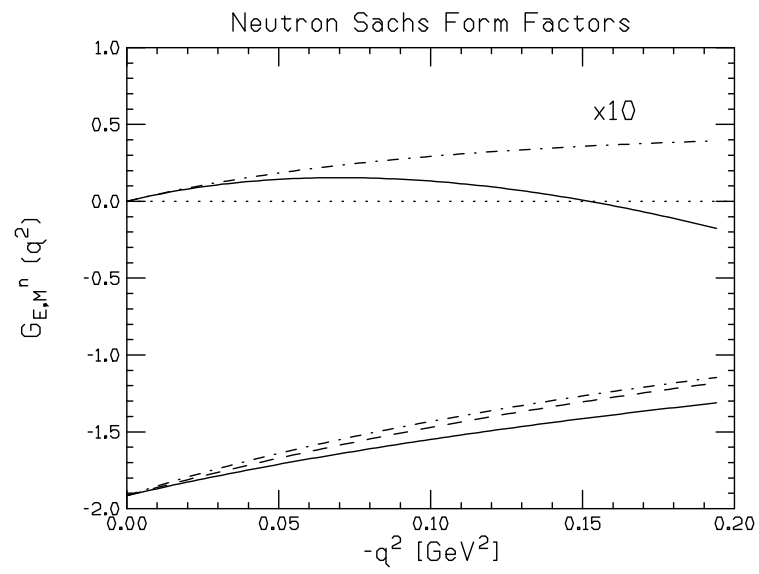


Figure 3b

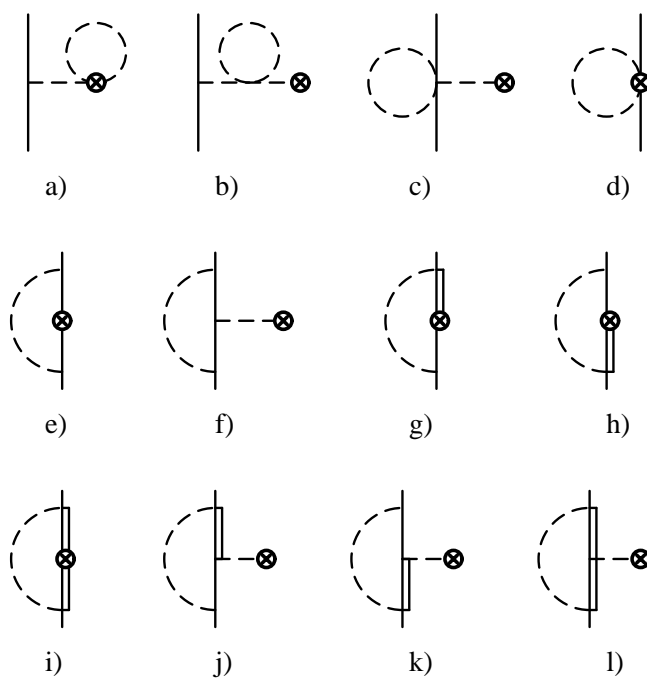


Figure 4